PHOTOMASK

BACUS—The international technical group of SPIE dedicated to the advancement of photomask technology.

Best Poster Runner Up — PUV18

Multiple Exposure on Single Blank for Electron-Beam Writer Characterization

André Eilert, Michael Finken, Christian Bürgel, Mark Herrmann, Ronald Hellriegel, Rico Nestler, Oliver Löffler, Frank Hübenthal, Rico Büttner, and Katja Steidel, Advanced Mask Technology Center GmbH & Co. KG, Rähnitzer Allee 9, 01109 Dresden, Germany

ABSTRACT

Electron-beam writer characterization is key to enable predictable product performance in a photomask shop. This is traditionally done by writing test patterns with one distinct tool on one blank. Within this article, we introduce a method that reduces uncertainty caused by variation of blanks and process parameters, by using multiple, subsequent electron-beam exposure steps with different same-of-a-kind tools. The method is demonstrated for the disentanglement of two of the most fundamental parameters in an e-beam tool, current density and blanker latency, which together determine the actual dose. Additional accuracy can be achieved by probing the same tool parameter with different methods, which is shown by comparing Critical Dimension Scanning Electron Microscopy of line-space patterns below the maximum shot size with Thin Film Optical Scatterometry of comparatively large pads. The multiple exposure method needs a proper correction of systematic effects caused by contact of exposed areas with air during mask transfer from one writer to another, which are presented and discussed.

1. Introduction

The production of a high-end photomask for 14nm node and below requires tight control of key performance indicators (KPI) such as critical dimension off-target (CDO), critical dimension uniformity (CDU), optical proximity correction signatures (OPC) and others. The integrated manufacture process consists thereby of several unit processes, e.g. formation of blank and resist, coat, bake, lithographic exposure with electrons, another bake, develop, etch and others. Since many of these unit processes have both direct impact on KPIs and indirect impact by influencing other unit processes (e.g. influence of resist profile on etch behavior), accurate tool and unit process characterization and monitoring is key for process partitioning and subsequently for predictable and stable product performance.

A typical unit process control consists of two to three levels: 1) control of tool and process parameters such as temperatures, flows, etc., 2) control by means of test masks with a layout that allows the characterization and partitioning of different influence factors, and 3) fine control based on product performance without influence factor partitioning. Particularly the partitioning of different influence factors, which is not only important for a stable process but also foundation of a mix-and-match approach,[1] can be a sophisticated task, as pointed out in the following example of key importance: the determination of the actual

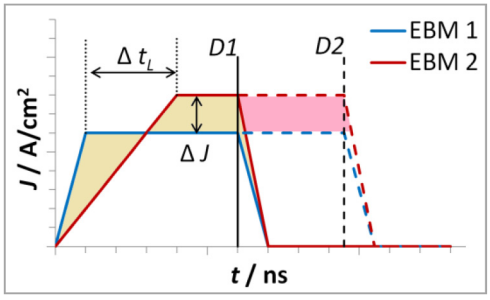

Figure 1. Illustration of dose application for one shot from 2 different electron-beam writers (EBM), linearly approximated. The actual dose is determined by the area under the curve. Whereas in case D1 *(solid line) the deviations in blanker latency* Δ*tL and current density* Δ*J compensate (yellow shaded area) to the same actual dose, EBM 2 applied additional dose (pink shaded area) in case* D2.

BACUS NEWS

APRIL 2019
VOLUME 35, ISSUE 4

TAKE A LOOK INSIDE:

SPIE.

10810-50

EDITORIAL

If your Head is not in the Cloud, it will be!

Patrick Martin, Applied Materials

I was privileged to attend a conference a few years back on the emerging markets for machine learning and artificial intelligence. It was a wonderful mix of venture capital, startups and industry heavy weights. What impressed me at the time was a talk that highlighted how machines learn and ultimately become extremely proficient at the tasks given to them. The talk presented the scenario where a machine was given the task of winning a computerized war game. At first, the machine was ineffective. It would get stuck in dead end barriers and get terminated by the enemy on short order but eventually it learned and easily defeated the enemy. The machine also taught another machine how to play which illustrated the possibility that knowledge is transferrable without direct human intervention. We do not really know how machines learn and infer. Scary in a sense, with sufficient scale, machines can learn in a week what took 10,000 years for humans to piece together. How do we really ensure we are ultimately in control if the machine becomes more intelligent than us other than by pulling the power plug?

Which brings me to the real topic on hand, machine learning for IC fabrication. It has many embodiments from tool operations where effectiveness can be measured against classic conditions such as tool utilization or cost of ownership as it relates to maintenance interval and consumables to big picture - design services in the cloud. The concept of creating a digital twin in a virtual state is fascinating especially as you can see it evolve and optimize to its environmental conditions provided by data from the real world. Some say we only analyze 4% of the data that is available hence, a fully equipped scaled hardware system can certainly look beyond that 4% to very complex multi-ordered interactions of data, that is, if it is affordable both in time and cost.

What “node” should we expect machines to take over and where in the nodal cycle? Design services are already in the cloud to some extent at 7nm and prior nodes but it is only a few percentages of the overall EDA revenue stream hence, the traditional models of the supply chain are still very healthy. Implementation leverages existing PDK’s hence it is an after effect of running full flow material to generate the design rule decks and it certainly benefits the startups that can leverage a friendlier cost structure to validate their IP. There is plenty of room to take the machine learning farther upstream into the design learning cycles especially with variability, performance matching, Design Technology Co-Optimization, System-Technology Co-Optimization, and more recently Design for Durability needs. How will it impact silicon content? Will it offer more flexibility to the design community? I would like to think so and with the diversification of technology needs in edge-based devices, it could really allow for some diversification without the disruption of having customized flows. Certainly, there is a lot of intense publicity and promotion around machine learning, it will be interesting to see how it evolves in time and the impact that it will have on our industry.

BACUS

N • E • W • S

BACUS News is published monthly by SPIE for BACUS, the international technical group of SPIE dedicated to the advancement of photomask technology.

Managing Editor/Graphics Linda DeLano

SPIE Sales Representative, Exhibitions, and Sponsorships Melissa Farlow

BACUS Technical Group Manager Marilyn Gorsuch

SPIE.

P.O. Box 10, Bellingham, WA 98227-0010 USA
Tel: +1 360 676 3290
Fax: +1 360 647 1445
SPIE.org
help@spie.org

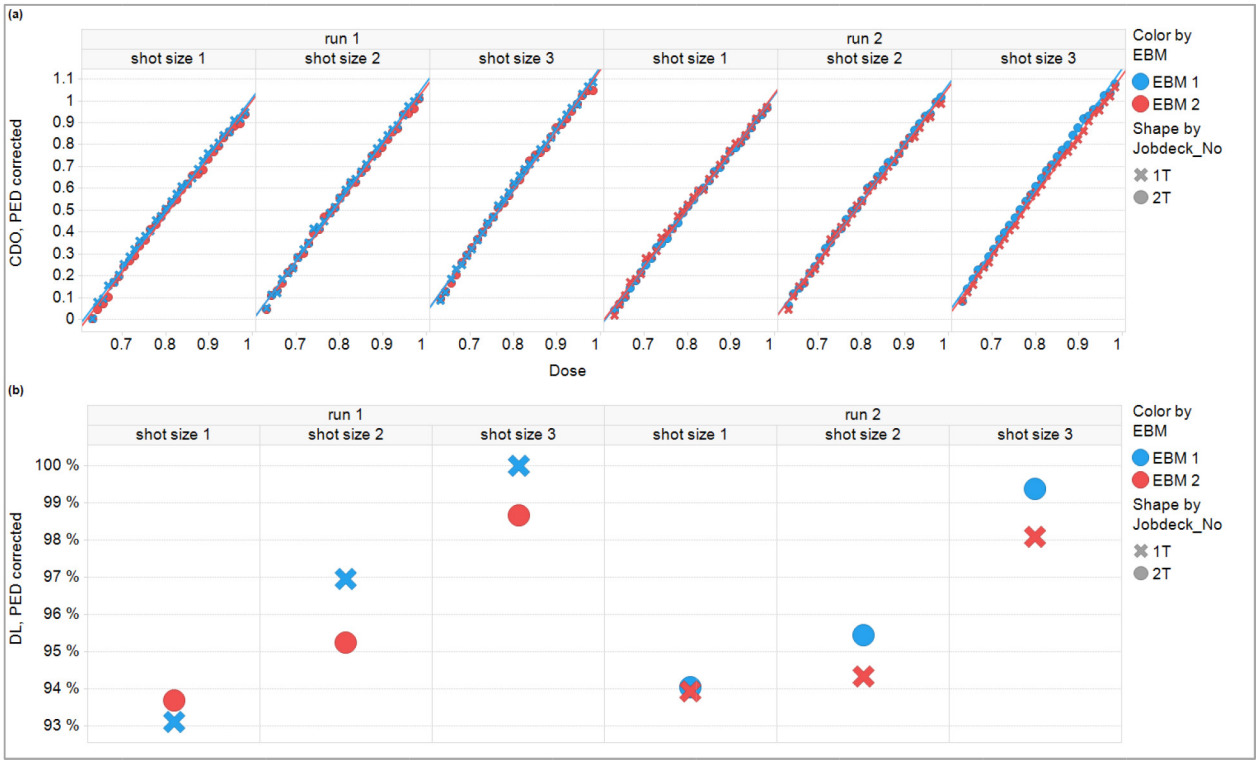

Figure 2. Comparison of dose latitudes from two EBMs in two separate runs, each with two subsequent exposure steps. (a) CDO of 1:1 dense features after Post-Exposure-Delay (PED) correction for three shot sizes all below the maximum shot size, with linear fits, (b) dose latitudes DL.

dose applied in the resist during the electron-beam write process.

The actual dose applied with one shot of a variable shaped electron-beam writer depends on blanker performance and current density. Both can be characterized in-line with a Faraday cup and subsequent electrometer, and current density variations are typically compensated during the write process. The second level of control consists of a test mask which measures the actual dose independently of any other tool and process parameter, and partitions between blanker performance and current density. In a first approximation one could use the dose-to-size as measure of actual dose, however, dose-to-size is strongly dependent on both tool parameters of the writer itself such as shot size and other process parameters such as PEB/Dev/Etch-conditions or metrology offset. A better approximation can be gained by measuring relative CD differences on a test mask, e.g. density, defocus or dose dependent CD (dose latitude), which reduces or eliminates few of the above mentioned effects like a metrology offset. However, those measurements alone still suffer from accuracy limitations: for instance the dose latitude, ideally a measure of current density, has shown to depend on the shot size. This phenomenon could be explained by coulomb interactions in the column leading to a shotsize dependent focal point. Consequently, any (relative) CD measurement is affected by this and similar effects,[2] and additional partitioning accuracy can only be gained by comparing to other properties than CD, such as dose-dependent resist thickness of large pads much bigger than the maximum shot size (contrast curves). These, in contrast, do not depend on the focal point, however, they are influenced by a shot offset which affects the total number of electrons, either by slightly overlapping shots in case of a positive offset or small gaps between the shots in case of a negative offset. Since in return the shot offset influence on the dose latitude is negligible for shot sizes more than ~3 times bigger than the blur, a comparison of contrast curves with dose latitude measurements significantly increases partitioning accuracy for actual dose determination.

Even though these methods increase partitioning accuracy significantly, they still depend on external material and process parameters which affect different observables similarly. Assume a resist threshold variation across different blanks: Since the resist threshold is the detector for both dose latitude and dose-dependent resist thickness, any variation in resist threshold will be misinterpreted as variation in actual dose.

We are able to reduce the remaining influence of material and process variation largely by comparing test structures written with different writers on the same blank. This method increases the partitioning accuracy significantly. Within this paper, this is demonstrated for actual dose determination and blanker latency characterization. The influence from mask exposure to atmosphere between the subsequent write steps needs to be characterized and corrected which is described in an extra section.

2. Actual Dose

The actual dose which is applied to the resist during the electron-beam write process is determined by current density J and blanker latency t_L. Figure 1 illustrates a hypothetical, linearly idealized situation where EBM 1 shows a faster blanker response and EBM 2 a higher current density. In case of application of dose *D1*, both effects compensate each other and thus both EBMs apply the same actual dose. However, in case of dose *D2*, the prolonged blanker opening time leads to a dose deviation resulting in a higher dose from EBM 2 (pink shaded area). Since the deviation of actual dose between *D1* and *D2* is independent of Δt_L in case of sufficiently long shot durations, dose latitude (*DL*) and contrast curves can be used to measure ΔJ. Note that there is an in-line J measurement using a Faraday cup and subsequent electrometer in the tool, however, an independent method is necessary to cover small drifts for instance in cup efficiency (e.g. changed secondary electron generation caused by a changed work function) or in electrometer sensitivity.

The *DL* of 1:1 dense features was measured with Critical Dimension

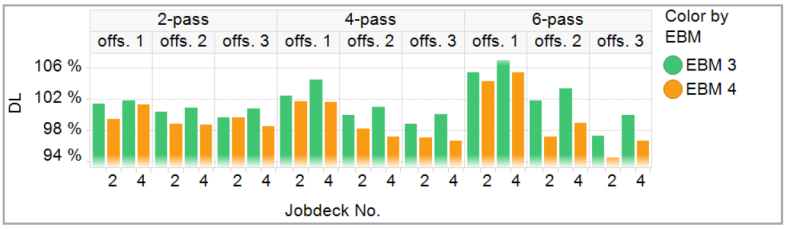

Figure 3. Measured dose latitudes from an experiment with four subsequent litho exposure steps in the order EBM 3 – EBM 4 – EBM 3 – EBM 4. A time offset was added to each shot whereas offset 2 was twice and offset 3 three times as long as offset 1. The 1:1 dense structures were written 2-, 4- and 6-pass mode.

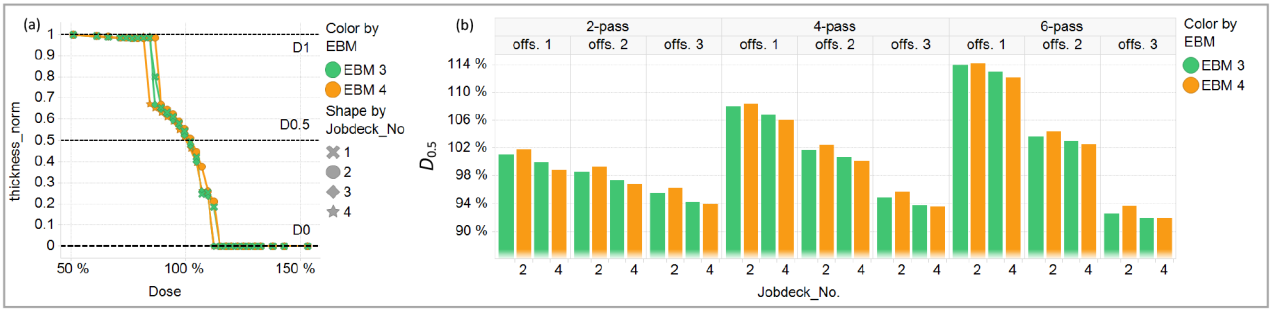

Figure 4. (a): Contrast curves from EBMs 3 and 4 written 4-pass with offset 2 using the same experimental setup as in Figure 3. (b): $D_{0.5}$ values.

Scanning Electron Microscopy in positive chemically amplified resist (Pcar RCD). Thereby, *DL* is the linear slope of CD vs. set dose D_{set},

$$CD = DL \bullet D_{set} + y_0. \quad (1)$$

Other descriptions such as a logarithmic approach improved fitting residuals but resulted in less stable *DL* determination. In case of drift of cup efficiency or electrometer sensitivity, the actual dose differs from the set dose linearly by the factor α within a first approximation. By comparing two EBMs 1 and 2, one can deduct

$$\alpha_1/\alpha_2 = DL_1/DL_2 \quad (2)$$

Thus, the ratio of dose latitudes from two EBMs is a measure of actual dose ratio, and is a lot more stable towards other material and process parameters than the dose latitude measured on a test mask exposed with just one EBM alone, as shown in Figure 2. In Figure 2(a), the CDO for 3 target CD values from 2 separate runs is fitted linearly. Post-Exposure-Delay (PED) correction as described in section 4 was applied. Both runs consisted of two subsequent litho exposure steps with two same-of-a-kind tools, whereas the order of EBMs was inversed between both runs, i.e. in run 1, EBM 1 wrote test pattern “1T” first and EBM 2 wrote test pattern “2T” second, whereas in run 2, EBM 2 wrote test pattern “1T” first and EBM 1 wrote test pattern “2T” second.

Figure 2(b) displays *DL*s as percentage from the maximum value. For both EBMs, the dose latitude increases with shot size, which is assigned to shot-size dependent focus variations causing limited partitioning accuracy, which can only be solved by a second, focus-independent method such as the measurement of contrast curves on large pads. Since both EBMs possess slightly different column aberrations, observed by slightly different best focus values and skews of Bossung plots,[3-5] the actual dose ration between both EBMs appears to be shot-size dependent.

Neglecting the focus effect in a first assumption, EBM 2 shows a reduced actual dose by ~1.5 % for shot sizes 2 and 3. It would be impossible to find this deviation without double exposure on a single blank, since absolute dose latitudes differ by up to 1.5 % between both runs. Taking longer time frames and several resist lots into account, which happens when several monitor masks are compared with each other, even deviations up to a few percent could be found, which shows the necessity of the multiple exposure approach.

For sufficient shot durations long enough to reach a plateau in current density, the actual dose difference observed in Figure 2 is caused by a beam current density deviation and not affected by blanker performance deviations (compare Figure 1). This hypothesis can be tested by artificially adding an offset to each shot, as displayed in Figure 3.

In this experiment, EBMs 3 and 4 were compared by writing four subsequent litho jobdecks on the same blank switching between both writers back and forth. The shot duration was varied by writing the same structures in 2-pass, 4-pass and 6-pass mode. Each *DL* was determined from seven dose steps only, with each dose step measured with less statistics than in Figure 2, which gives rise to a comparatively high level of random variation in dose latitude. Ideally, when the beam current on the sample reaches a plateau during the shot, the measured dose latitude is independent of the added time offset. This is roughly the case in 2-pass mode. By dividing the shot duration by 2 (4-pass) or 3 (6-pass), the added time offset starts having a larger influence on *DL* indicating that no plateau was gained during the shot. Since, in this case, an increase in dose leads to an increase in shot duration and *J*, the apparent *DL* is higher for shorter offset values. Consequently, this method should be used with as long shot durations as possible before resist heating effects start having significant influence. Blanker performance characterization is further evaluated in section 3.

The focus effect observed in Figure 2 can be suppressed by measuring contrast curves of large pads much bigger than the actual shot size. A set of exemplary contrast curves from 200x200 µm² pads is shown in Figure 4(a). Deviations from the textbook curve shape[6] are caused by model discontinuities of the Thin Film Optical Scatterometry (n&k) analysis. Because of that, the most stable parameter to describe actual dose is $D_{0.5}$, the dose where the model suggests 50 % of the initial resist thickness.

$D_{0.5}$ values were obtained for the same multipass and offset values as in the Figure 3 and are displayed in Figure 4(b). The data contain less noise and show stronger sensitivity towards multipass modes and time offset values compared to Figure 3, which is caused by the different underlying physics of the two measurement principles. Whereas contrast curves are a direct measure of actual dose, dose

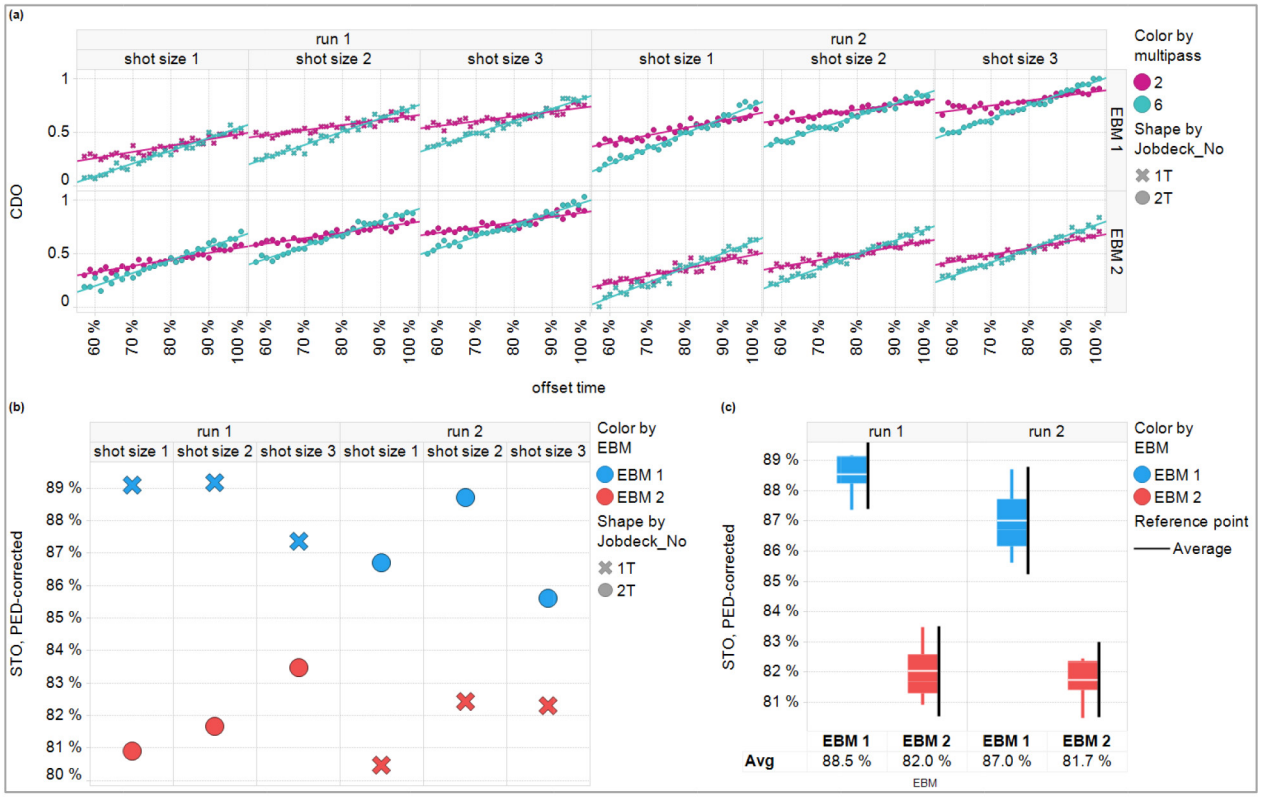

Figure 5. (a): CDO of 1:1 dense features in dependence of an extra offset time per shot, written in 2-pass and 6-pass mode. The intersection of both curves gives STO. *(b):* STO *after PED correction. (c): Box plot of (b).*

latitude measurements rely on blur of beam and process. Furthermore, $D_{0.5}$ is indirect proportional to actual dose: An EBM with a high actual dose shows a small $D_{0.5}$ on the same resist compared to an EBM with a lower actual dose. With that in mind, results from Figure 3 and 4 match to each other qualitatively indicating EBM 3 has a slightly higher actual dose than EBM 4. Quantitative deviations have multiple reasons such as difference in focus behavior (*DL*) or shot size ($D_{0.5}$) between the two EBMs. Consequently, the most accurate results can be gained by considering both methods and investigating and adjusting further parameters such as blanker latency.

3. Blanker Latency

The actual dose per shot differs from the calculated dose for instantaneous blanker performance by a certain amount depending on the blanker latency. This amount can be expressed as extra shot-time offset *STO* needed to apply the calculated dose. The *STO* can be measured by writing certain structure in dependence of an extra offset time per shot in varying multipass-modes as displayed in Figure 5. The experimental setup was the same as for Figure 2. Figure 5 (a) shows measured CDO values versus the offset time displayed as percentage from the maximum value, and linear fits for EBM 1 (top) and 2 (bottom). The offset time where the fits intersect, i.e. the time where CDO does not depend on the number of shots, gives the blanker's *STO*.

The *STO* values were PED-corrected as described in section 4 and are displayed in Figure 5 (b) and (c). EBM 2 showed a lower *STO* than EBM 1 by 6.5 percent points in run 1 and by 5.3 percent points in run 2. Obviously, the relative gain in accuracy compared to a single exposure experiment is lower than for the actual dose estimation shown in Figure 2, which originates form the fact that the intersection of two CDO curves is more stable towards external variations like resist sensitivity than the slop of a single CDO curve *DL*. However, the double exposure method still improves *STO* determination accuracy (*STO* values from run 2 are overall slightly below run 1 which suggests an external influence factor) and serves as internal outlier check: In case both EBMs show an unexpected *STO* value, the observation is likely to be driven externally, whereas in case of only one EBM showing an unexpected *STO*, it is likely to be EBM related.

The accuracy of *STO* determination as in Figure depends on several factors such as the actual opening function and shot-to-shot overlay. If the beam current on the sample reaches a plateau during the shots for both 2-pass and 6-pass modes, the actual opening function is of zero influence. However, in-line *J* measurements show that the blanker opening function rather follows an exponential function,

$$J(t) = J_{max}(1 - e^{-t/\tau}), \quad (3)$$

With the maximum beam current after full blanker opening J_{max} and the time constant τ. For this case one can show that there is no single *STO* parameter for all multipass modes and the intersections in Figure 5 (a) depend on the actual multipass choice. The extent of this effect increases the more the beam current does not reach a plateau. It can be tested by doing the experiment for at least 3 multipass modes, as simulated in Figure 6 for 2-, 4- and 6-pass mode, a shot time in case of zero offset of 1.2 and $\tau = 1$. In this case the lines do not intersect anymore in one point but rather form a triangle with apparent *STO* values between 0.26 and 0.48. Obviously, in this extreme case blanker latency cannot be corrected by a single offset value for all multipass modes and pattern densities but rather needs a more sophisticated correction. The size of the triangle can be used as quality assessment of the blanker response with respect to required shot durations.

The influence of the blanker opening function was tested in an experiment with four subsequent litho exposure steps in the order EBM 3 – EBM 4 – EBM 3 – EBM 4 as in Figure 3 and is displayed in Figure 7. CDO values in Figure 7 (a) are approximately directly proportional to

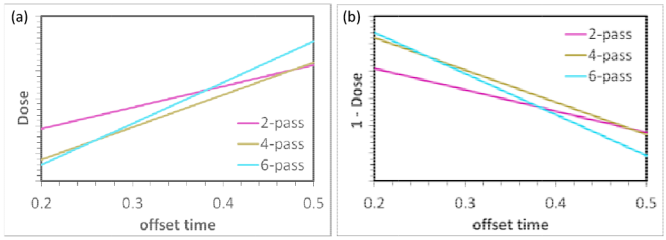

Figure 6. Dose simulation following Eq. (3) for 2-, 4- and 6-pass mode with a shot time in case of zero offset of 1.2 and τ = 1. (a) Dose versus offset time and (b) 1-dose versus offset time for illustration of $D_{0.5}$.

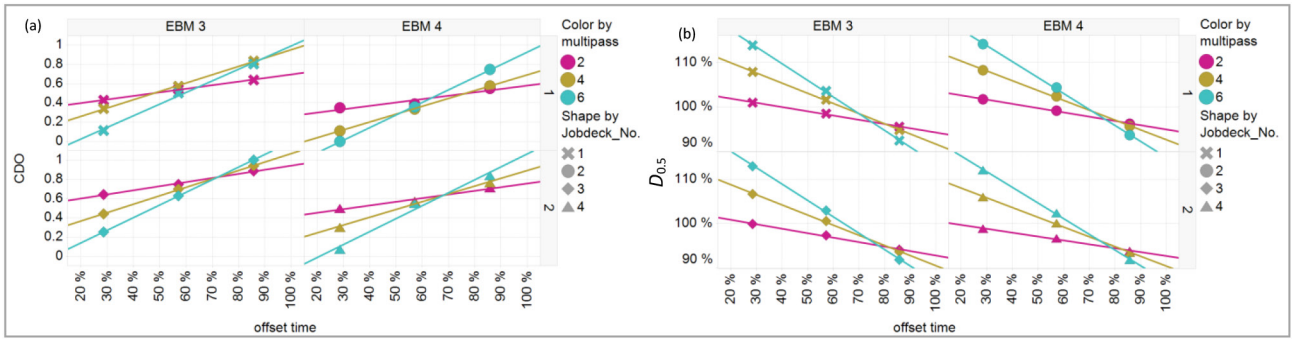

Figure 7. (a): CDO 1:1 dense features in dependence of an extra offset time per shot, written in 2-, 4- and 6-pass mode, from the same experimental setup as in Figure 3. (b): $D_{0.5}$ values from contrast curves.

dose values in Figure 6 (a). Apparently the influence of blanker opening function is comparatively small to the experimental accuracy. Whereas the third and fourth cycle (Jobdeck_No. 3 and 4) on EBM 3 and EBM 4, respectively, show one intersection point of all three multipass modes with 1% of the maximum applied offset time, Jobdeck_No. 2 follows the simulated effect of figure 6 (a) and Jobdeck_No. 1 shows the opposite behavior.

Another factor influencing *STO* accuracy from RCD is shot-to-shot overlay, adding extra CD to higher multipass modes. This can be circumvented by measuring contrast curves on large pads as displayed in Figure 7 (b). Similarly to the method evaluation in section 2, the contrast curve measurement seems to have a higher accuracy in this particular example as the influence of the blanker opening function, illustrated in Figure 6 (b), is clearly visible in all four cases. *STO* values from contrast curves are on average ~10 percent points higher than from the RCD measurement, and in this particular case, the visibility of the blanker opening function gives the contrast curve measurement a higher reliability.

4. Post Exposure Delay

The setup at hand compares test structures from two or more EBMs written on a single blank. The partly exposed blank is transferred in a pod in air between the subsequent litho steps which causes systematic effects that need to be corrected. Since production data of the investigated resists suggest that a few hours delay time in vacuum after exposure is of comparatively small influence and since write durations of the same jobdeck on same-of-a-kind tools is very comparable, we use no extra correction for the delay time in vacuum, sometimes referred as vacuum delay.

In contrast, delay time in air, sometimes referred to PEB Delay,[7] turned out to be of significant influence. It can be speculated that water vapor is the main driving force for this effect (apart from others such as amine contamination), since it is supposed to dramatically increase acid mobility via the GROTTHUS mechanism. Considering a relative humidity of 30 % corresponding to 7.5 mbar partial pressure and a sticking coefficient of ~0.2, it takes less than 10^{-6} seconds to deposit 1 monolayer of water on the resist.[8] A 100 nm resist has a thickness corresponding to ~300 layers of water, and the amount of water in the pod atmosphere is more than one order of magnitude higher than needed to fully hydrate the resist assuming a volume ratio water/resist of ~0.5. Thus, even for limited diffusion, it can be assumed that the resist is instantaneously hydrated when it is brought in contact with air.

Post Exposure Delay was characterized by two subsequent litho steps on the same writer with defined exposure to air in between. Exemplary results for an nCAR resist are shown in Figure 8 (a). Here, the CD_{clear} difference between patterns from the first and the second jobdeck is denoted as CD_{clear} change, i.e. the influence of post exposure delay to the patterns written in the first jobdeck. In case of an ideal experiment, i.e. a stable EBM and zero vacuum delay, the CD_{clear} change from zero air time is zero. With increasing air time, clear structures get bigger, which can be explained by acid neutralization as dominant factor within this time regime, e.g. caused by reaction with the quencher in the resist. Typical air times of experimental runs are 30 % of the maximum applied time in Figure 8 (a), and variation is small enough for effective correction. However, we were also interested to see what happens when keeping the mask on purpose ~3 times longer in air between the litho steps than relevant for normal operation. Obviously, a second effect became dominant which decreases CD_{clear}. It is a reasonably hypothesis that from zero to ~30 % air time, acid diffuses out of the exposed area and gets quenched, which increases CD_{clear}. After a certain time, quencher concentration close to the exposed area gets low and additional acid diffusion from inner parts of the exposed area effectively reduce CD_{clear}.

Interestingly, an apparent dose decrease due to exposure to air for typical air times can also be seen in contrast curve measurements. Figure 8 (b) is based on the same data as Figure 7 (b). All linear fits of $D_{0.5}$ vs. offset time are shifted upwards parallel to the y-axis for longer air time (= lower Jobdeck_No.), which corresponds to an effective dose decrease. Since the dose regime for contrast curves is much smaller than for the RCD patterns, it is imaginable that the neutralization reaction between acid and quencher within a pad gets enhanced due to the presence of water, effectively increasing $D_{0.5}$. Furthermore,

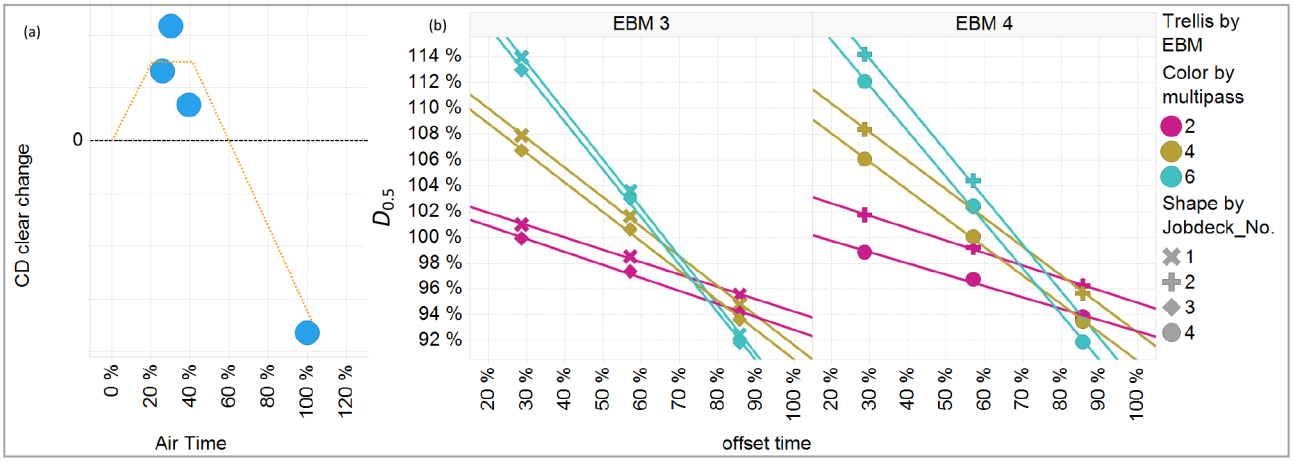

Figure 8. (a) CDO clear change as function of air time between litho exposure steps for an nCAR resist. The orange dotted line serves as guide to the eye. (b): $D_{0.5}$ values from contrast curves and linear fits.

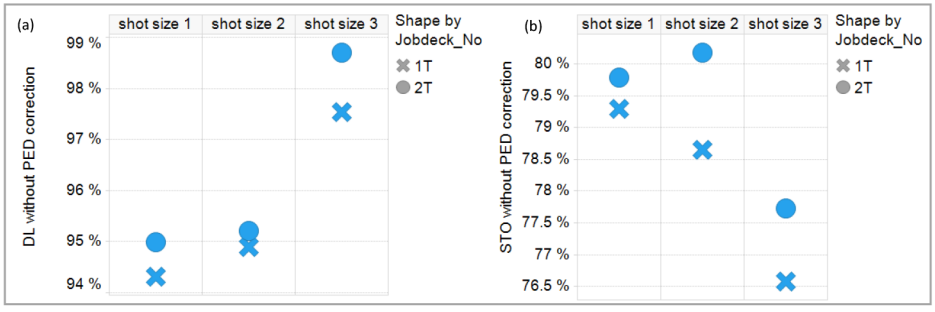

Figure 9. Effect of Post Exposure Delay on STO *(a) and* DL *determination (b) from RCD for a typical air time. Jobdecks 1T and 2T were written with the same EBM tool.*

by comparing the intersections of corresponding multipass curves, a slight decrease of apparent STO due to exposure to air can be seen (i.e. intersections of lower jobdeck numbers occur at lower offset times).

There is also a small but significant, systematic effect of post exposure delay to *DL* and *STO* from RCD measurements (Figure 9). The effect on both parameters is of similar relative magnitude compared to the overall experimental accuracy, given by shot-size dependent variations. Furthermore, qualitative systematic effects are the same as for contrast curve measurements, i.e. the apparent actual dose and *STO* are lower for the lower jobdeck number.

5. Conclusion

The use of a multiple exposure method was demonstrated for the characterization of actual dose and blanker latency of variable shaped electron-beam writers used in a photomask shop. The method shows many advantages over the traditional single exposure approach which are: 1) higher accuracy due to better distinction between tool-related and external influence factors, 2) intrinsic outlier check, 3) lower cost and 4) faster results, compared to the same amount of information from multiple single-exposed blanks. Oppositely, the method needs a decent one-time investment for proper post exposure delay correction. The gain in accuracy depends on the stability of the investigated parameter towards external influence factors. As an example, actual dose determination shows a large accuracy gain since the investigated parameter depends directly on the resist threshold, whereas the accuracy gain for blanker latency characterization is comparatively small. Further accuracy can be achieved by combining different methods which probe properties that react independently upon external variations, such as critical dimension scanning electron microscopy of test structures on a ~100 nm scale versus dose-dependent resist thickness measurements of 200 µm large pads.

6. References

[1] Frangen A., Jakob R., and Kubis M., "Mask manufacturing mix-and-match in frontend wafer processing," **Proc. SPIE 5567,** 116 (2004).

[2] Park S., Park J., Lee B., Choi J., Shin I.K., and Jeon C.-U., "Requirements of the e-beam shot quality for mask patterning of the sub-1X device," **Proc. SPIE 9777,** 977716 (2016).

[3] Keil K. and Hauptmann M., "Resolution and total blur: Correlation and focus dependencies in e-beam lithography," *J. Vac. Sci. Technol. B 27,* 2722 (2009).

[4] Bossung J. W., "Projection Printing Characterization," **Proc. SPIE 100,** 80 (1977).

[5] Keil K., Choi K.-H., Hohle C., Kretz J., Lutz T., Bettin L., Boettcher M., Hahmann P., Kliem K.-H., Schnabel B., Irmscher M., and Sailer H., "Determination of best focus and optimum dose for variable shaped e-beam systems by applying the isofocal dose method," *Microelectron. Eng. 85,* 778 (2008).

[6] Steidel K., "Untersuchung der Auflösungsgrenzen eines Variablen Formstrahlelektronenstrahlschreibers mit Hilfe chemisch verstärkter und nicht verstärkter Negativlacke", Fraunhofer Verlag, Stuttgart (2011).

[7] Smith M. A., Vitale S. A., Fedynyshyn T. H., Cook M. T., Maldonado J., Shapiro D., and Rothschild M., "High-resolution, high-throughput, CMOS-compatible electron-beam patterning," **Proc. SPIE 10146,** 10146H (2017).

[8] Kolasinski K. W., "Surface Science: Foundations of Catalysis and Nanoscience", 3rd. Ed., John Wiley & Sons Ltd, Chichester (2012).

BACUS N • E • W • S

Sponsorship Opportunities

Sign up now for the best sponsorship opportunities

Photomask Technology + EUV Lithography 2019

Contact: Melissa Farlow,
Tel: +1 360 685 5596; **melissaf@spie.org**

Advanced Lithography 2020

Contact: Teresa Roles-Meier,
Tel: +1 360 685 5445; **teresar@spie.org**

Advertise in the BACUS News!

The BACUS Newsletter is the premier publication serving the photomask industry. For information on how to advertise, contact:

Melissa Farlow,
Tel: +1 360 685 5596
melissaf@spie.org

BACUS Corporate Members

Acuphase Inc.
American Coating Technologies LLC
AMETEK Precitech, Inc.
Berliner Glas KGaA Herbert Kubatz GmbH & Co.
FUJIFILM Electronic Materials U.S.A., Inc.
Gudeng Precision Industrial Co., Ltd.
Halocarbon Products
HamaTech APE GmbH & Co. KG
Hitachi High Technologies America, Inc.
JEOL USA Inc.
Mentor Graphics Corp.
Molecular Imprints, Inc.
Panavision Federal Systems, LLC
Profilocolore Srl
Raytheon ELCAN Optical Technologies
XYALIS

Industry Briefs

Semiconductor Engineering - Mixed Outlook For Silicon Wafer Biz

By **Mark LaPedus,** Semiconductor Engineering

After a period of record growth, the silicon wafer industry is off to a slow start in 2019 and facing a mixed outlook. 200mm silicon wafer supply remains tight. But demand for 300mm silicon wafers is cooling off in some segments, causing supply to move toward equilibrium after a period of shortages. On average, though, silicon wafer prices continue to rise despite the slowdown.

This affects the entire semiconductor industry because silicon wafers are a fundamental part of the business. Every chipmaker needs to buy them in one size or another. Silicon wafer vendors produce and sell bare or raw silicon wafers to chipmakers, who in turn process them into chips.

But 2019 is different than past years. From 2016 to 2018, silicon wafer makers saw booming demand, causing tight supply and high prices for wafers. In 2019, though, the IC market is slowing, which impacts the silicon wafer industry on various fronts. Worldwide capacity utilization for 300mm wafers will hover around 95% in 2019, compared to 100% in 2018, according to Sumco, a silicon wafer supplier.

https://semiengineering.com/mixed-outlook-for-silicon-wafer-biz/

Sensors Online

By **Mathew Dirjish**

According to Gartner researchers, worldwide semiconductor revenue totaled $476.7 Billion in 2018, a 13.4% increase from 2017. Memory strengthened its position as the largest semiconductor category, accounting for 34.8% of total semiconductor revenue, up from 31% in 2017.

The largest semiconductor supplier, Samsung Electronics, increased its lead as the No. 1 vendor due to the booming DRAM market.

The combined revenue of the top 25 semiconductor vendors increased by 16.3% during 2018 and accounted for 79.35% of the market, outperforming the rest of the market, which saw a milder 3.6% revenue increase. Major memory vendors that performed strongly in 2018 include SK hynix — driven by DRAM, and Microchip Technology — due to its acquisition of Microsemi. As the market for smartphones and tablets continues to saturate, application processor vendors must seek adjacent opportunities in wearables, Internet of Things (IoT) endpoints and automobiles.

Circuit Insight - The 5G Future Is Almost Here

The 5G future is arriving faster than many had predicted. But, for the struggling telecom industry, it still can't arrive fast enough. The mobile telecom industry has left behind the era of easy growth, driven by smartphone and tablet adoption. And the anticipated new era of growth based on innovations like virtual reality and the Internet of Things hasn't yet picked up the slack.

But, in recent months, the mood among telecom leaders, is imbued with newfound optimism. Already, momentum is building for actual rollouts and there is hope that 5G networks will soon unleash an avalanche of investment and inspire a wave of new services that profoundly changes the world, while also returning the telecom industry to a new era of prosperity.

So far, U.S. telecom companies have spent over $60 billion for 5G-compatible segments of the electromagnetic spectrum in Federal Communications Commission spectrum auctions. Telecom companies in Germany, India, and Canada have also heavily invested in securing spectrum rights.

China Mobile and Japan's NTT Docomo are targeting 2020 for their 5G launch. On the chip side, Qualcomm has been making an aggressive push, including deals with 19 phone makers and 18 carriers for 5G. (Qualcomm's 5G traction has also made it the target of a hostile takeover bid from Broadcom.) And Intel has partnered with PC makers to develop 5G-enabled laptops for 2019.

http://www.circuitinsight.com/programs/55315.html

Join the premier professional organization for mask makers and mask users!

About the BACUS Group

Founded in 1980 by a group of chrome blank users wanting a single voice to interact with suppliers, BACUS has grown to become the largest and most widely known forum for the exchange of technical information of interest to photomask and reticle makers. BACUS joined SPIE in January of 1991 to expand the exchange of information with mask makers around the world.

The group sponsors an informative monthly meeting and newsletter, BACUS News. The BACUS annual Photomask Technology Symposium covers photomask technology, photomask processes, lithography, materials and resists, phase shift masks, inspection and repair, metrology, and quality and manufacturing management.

Individual Membership Benefits include:

- Subscription to BACUS News (monthly)
- Eligibility to hold office on BACUS Steering Committee

spie.org/bacushome

Corporate Membership Benefits include:

- 3-10 Voting Members in the SPIE General Membership, depending on tier level
- Subscription to BACUS News (monthly)
- One online SPIE Journal Subscription
- Listed as a Corporate Member in the BACUS Monthly Newsletter

spie.org/bacushome

CALENDAR

2019

Photomask Japan
16-18 April 2019
PACIFICO Yokohama
Yokohama, Japan
photomask-japan.org

The 35th European Mask and Lithography Conference, EMLC 2019
17-19 June 2019
Hilton Hotel Dresden
Dresden, Germany

SPIE Photomask Technology + EUV Lithography
15-19 September 2019
Monterey Conference Center and
Monterey Marriott
Monterey, California, USA

2020

SPIE Advanced Lithography
23-27 February 2020
San Jose Marriott and
San Jose Convention Center
San Jose, California, USA

SPIE is the international society for optics and photonics, an educational not-for-profit organization founded in 1955 to advance light-based science, engineering, and technology. The Society serves nearly 264,000 constituents from 166 countries, offering conferences and their published proceedings, continuing education, books, journals, and the SPIE Digital Library in support of interdisciplinary information exchange, professional networking, and patent precedent. SPIE provided more than $4 million in support of education and outreach programs in 2018. **spie.org**

SPIE.
International Headquarters
P.O. Box 10, Bellingham, WA 98227-0010 USA
Tel: +1 360 676 3290
Fax: +1 360 647 1445
help@spie.org • **spie.org**

Shipping Address
1000 20th St., Bellingham, WA 98225-6705 USA

Managed by SPIE Europe
2 Alexandra Gate, Ffordd Pengam, Cardiff,
CF24 2SA, UK
Tel: +44 29 2089 4747
Fax: +44 29 2089 4750
spieeurope@spieeurope.org • **spieeurope.org**

You are invited to submit events of interest for this calendar. Please send to lindad@spie.org; alternatively, email or fax to SPIE.